Cr^{4+} in Tetrahedral Coordination of Oxidic Solids: A Spectroscopic and Structural Investigation

D. Reinen,*,† U. Kesper,† M. Atanasov,‡ and J. Roos†

Fachbereich Chemie und Zentrum für Materialwissenschaften der Philipps-Universität, Hans-Meerwein-Strasse, D-35032 Marburg, Germany, and Institute of General and Inorganic Chemistry, Bulgarian Academy of Sciences, Bl.11, Sofia 1113, Bulgaria

Received May 10, 1994[⊗]

Various oxidic solids with chromium(IV) in tetrahedral sites have been synthesized, predominantly without impurities of chromium in other oxidation states, and spectroscopically investigated. The d−d spectra show the typical features of a d^2 cation in distorted tetrahedral coordination and could be fitted by utilizing AOM calculations on the basis of the geometry of the host tetrahedra with the parameter set $\Delta \simeq 9650$ cm^{-1}, $B_{et} \simeq 480$ cm^{-1} ($\beta_{et} \simeq 0.47$), $C/B = 4.2$. The EPR spectra usually exhibit only one exchange-averaged signal; the fine structure is only occasionally resolved.

Introduction

The oxidation state of +IV for chromium is rather unstable, and only few oxidic chromium(IV) compounds are known and fully characterized.[1] In oxidic coordination it is usually found with a tetrahedral geometry, one of the very few exceptions being CrO_2 with the rutile structure. Well established are the compounds $Cr(O^tBu)_4$[2] and $Cr(OCHBu_3)_4$.[3] While the former was spectroscopically characterized [$\Delta = 9430$ cm^{-1}, $B = 795$ cm^{-1}], a crystal structure determination was performed in the latter case. From the reported average bond length of 1.77 Å an ionic radius of 0.42 Å (with $r(O^{2-}) = 1.35$ Å)[4] is estimated, in rather good agreement with the literature value.[4] Three further oxidic Cr(IV) compounds Ba_3CrO_5 and $M^{II}_2CrO_4$ [M^{II} = Ba, Sr] are known, of which Ba_2CrO_4 was investigated twice—by single-crystal X-ray analysis (space group $Pb2_1a$, No. 33)[5] and by powder neutron diffraction analysis (space group *Pnma*, No. 62).[6] It crystallizes in a β-K_2SO_4-related structure, and an average Cr−O spacing of 1.76 Å is found.[6] The bond distances between 1.67 and 1.80 Å and the bond angles (105° < 2θ < 114°) indicate rather distorted tetrahedra, however. In Ba_3CrO_5, the CrO_4 tetrahedra are almost regular with Cr−O bond lengths of 1.77 Å, identical with those in $Cr(OCHBu_3)_4$.[3] A small angular tetragonal elongation induced by packing effects in the Cs_3CoCl_5-type lattice is present. Sr_2CrO_4 crystallizes in a β-K_2SO_4-type structure with a doubled *b* unit cell axis. It contains two crystallographically independent Cr(IV) tetrahedra,[7] which are again distorted—in particular site 2 is extremely irregular, with bond angles varying between 97 and 126° and Cr−O spacings between 1.67 and 1.95 Å. The two polyhedra are characterized by different average Cr−O spacings of 1.80 and 1.85 Å, respectively. It is not clear why Cr(IV) adopts distorted geometries of this kind and, particularly, why it occupies different sites with widely varying extents of distortion, because obvious electronic reasons are not present for an orbitally nondegenerate $^3A_2$ ground state in T_d.

The spectroscopic evidence for tetrahedral Cr(IV) in oxidic solids is scarce. Since the discovery of Cr(III)-based tunable lasers in the near IR (7435−8570 cm^{-1}),[8-10] a great deal of spectroscopic work, both optical and EPR, has been performed to identify laser-active centers.[11-17] The best studied chromium-doped forsterite (Mg_2SiO_4) is claimed to contain Cr^{4+} besides Cr^{3+} though clear spectroscopic evidence is not present, mainly due to the overlap of transitions from various chromium species in the host lattice. In the first papers of Petricevic et al. the lasing transitions were ascribed to Cr^{3+} whereas later studies assigned it to Cr^{4+}.[11-15] While Cr^{3+} (and Cr^{2+}) ions seem to enter the octahedral Mg^{2+} sites, Cr^{4+} is expected to replace Si^{4+}. Only recently were the spectra analyzed and assigned by means of fluorescence and site-selective excitation spectroscopy.[15] The reported Cr^{4+} ligand field parameters of $\Delta \simeq 10\,000$ cm^{-1}, $B = 860$ cm^{-1}, and $C/B \simeq 4.9$ are similar to those reported for $Cr(O^tBu)_4$,[2] the Δ value being well in accord with a tetrahedral coordination, for example in comparison with Mn(V) in a

† Philipps-Universität.
‡ Bulgarian Academy of Sciences.
⊗ Abstract published in *Advance ACS Abstracts,* November 15, 1994.

(1) Nag, K.; Bose, S. N. *Struct. Bonding* **1985**, *63*, 153.
(2) Alyea, E. C.; Basi, J. S.; Bradley, D. C.; Chisholm, M. H. *J. Chem. Soc. A* **1971**, 772.
(3) Bochmann, M.; Wilkinson, G.; Young, G. B.; Hursthouse, M. B.; Abdul Malik, K. M. *J. Chem. Soc., Dalton Trans.* **1980**, 1863.
(4) Shannon, R. D. *Acta Crystallogr., Sect. A* **1976**, *32*, 751.
(5) Mattausch, Hj.; Müller-Buschbaum, Hk. *Z. Anorg. Allg. Chem.* **1974**, *07*, 129.
(6) Liu, G.; Greedan, J. E.; Gong, W. *J. Solid State Chem.* **1993**, *105*, 78.
(7) Wilhelmi, K.-A. *Ark. Kemi* **1966**, *26*, 157.
(8) Petricevic, V.; Gayen, S. K.; Alfano, R. R.; Yamagishi, K.; Anzai, H.; Yamaguchi, K. *Appl. Phys. Lett.* **1988**, *52*, 1040.
(9) Petricevic, V.; Gayen, S. K.; Alfano, R. R.; Yamagishi, K.; Moriya, K. In *Proceedings of the International Conference on Lasers '87*; Duarte, F. J., Ed.; STS: McLean, VA, 1988; p 423.
(10) Petricevic, V.; Gayen, S. K.; Alfano, R. R. *Photonic Spectra* **1988**, *22*, 95.
(11) Petricevic, V.; Gayen, S. K.; Alfano, R. R. *Appl. Phys. Lett.* **1988**, *53*, 2590.
(12) Verdun, H. R.; Thomas, L. M.; Andrauskas, D. M.; McCollum, T.; Pinto, A. *Appl. Phys. Lett.* **1988**, *53*, 2593.
(13) Alfano, R. R.; Petricevic, V.; Seas, A. *Proc. Int. Conf. Lasers* **1989**, 441.
(14) Petricevic, V.; Gayen, S. K.; Alfano, R. R. In *OSA Proceedings on Tunable Solid State Lasers*; Shand, M. L., Jenssen, H. P., Eds.; North Falmouth: Cape Cod, MA, 1989; Vol. 5, p 77.
(15) Jia, W.; Liu, H.; Jaffe, S.; Yen, W. M.; Denker, B. *Phys. Rev. B* **1990**, *43*, 5234.
(16) Moncorge, R.; Cormier, G.; Simkin, D. J.; Capobianco, J. A. *IEEE J. Quantum Electron.* **1991**, *27*, 114.
(17) Whitmore, M. H.; Sacra, A.; Singel, D. J. *J. Chem. Phys.* **1993**, *98*, 3656.
(18) Smyth, J. R.; Hazen, R. M. *Am. Mineral.* **1973**, *58*, 588.

0020-1669/95/1334-0184$09.00/0

Table 1. Structural Properties (Unit Cell Parameters (Å), Space Group, Structure Type, Bond Lengths (Å), and Bond Angles (deg)] of Ba_2CrO_4, Ba_3CrO_5, and Various Host Compounds Used for Cr^{4+} Incorporation

γ-Ca_2GeO_4[22]	$a = 6.787$	*Pnma*	olivine	Ge−O1 = 1.748	O1−O2 = 115.3
	$b = 5.239$	No. 62		Ge−O2 = 1.777	O1−O3 = 115.9[2×]
	$c = 11.397$			Ge−O3 = 1.785[2×]	O2−O3 = 101.8[2×]
					O3−O3′ = 104.3
Ba_3CrO_5[6]	$a = 7.303$	*I4/mcm*	Cs_3CoCl_5	Cr−O = 1.769[4×]	O−O′ = 104.9[2×]
	$c = 11.670$	No. 140			O−O′ = 111.8[4×]
$Ba_2MgGe_2O_7$[25]	$a = 8.347$	$P\bar{4}2_1m$	akermanit	Ge−O1 = 1.732[2×]	O1−O1′ = 103.3
	$b = 5.554$	No. 113		Ge−O2 = 1.722	O1−O2 = 118.7[2×]
				Ge−O3 = 1.794	O1−O3 = 102.2[2×]
					O2−O3 = 112.7
Ba_2CrO_4[6,a]	$a = 5.914$	*Pnma*	β-Ca_2SiO_4	Cr−O1 = 1.745	O1−O2 = 120.7
	$b = 7.629$	No. 62		Cr−O2 = 1.674	O1−O3 = 109.0[2×]
	$c = 10.464$			Cr−O3 = 1.801[2×]	O2−O3 = 105.5[2×]
					O3−O3′ = 106.2
Ca_2PO_4Cl[28]	$a = 6.185$	*Pbcm*	spodiosite	P−O1 = 1.550[2×]	O1−O1′ = 107.3
	$b = 6.983$	No. 57		P−O2 = 1.532[2×]	O2−O2′ = 107.8
	$c = 10.816$				O1−O2 = 113.6[2×]
					O1−O2′ = 107.3[2×]
Ca_2VO_4Cl[29]	$a = 6.311$	*Pbcm*	spodiosite	V−O1 = 1.711[2×]	O1−O1′ = 107.0
	$b = 7.140$	No. 57		V−O2 = 1.703[2×]	O2−O2′ = 105.6
	$c = 11.052$				O1−O2 = 116.3[2×]
					O1−O2′ = 105.9[2×]
$Ca_5(PO_4)_3Cl$[27,b]	$a = 9.628$	$P2_1/b$	apatite	P−O1 = 1.533	O1−O2 = 111.3
	$b = 2a$	No. 14		P−O2 = 1.544	O1−O3 = 111.9[2×]
	$c = 6.764$			P−O3 = 1.531[2×]	O2−O3 = 106.5[2×]
	$c = 120°$				O3−O3′ = 107.7

[a] The structure determination[5] claims a C_1 symmetry of the CrO_4 polyhedron, with the equivalence of the two O3 atoms removed. [b] Bond distances and angles are averaged over the inequivalent and slightly different O3 and O3′ positions, thus referring to the higher symmetry (hexagonal, space group $P6_3/m$, No. 176) description of the apatite structure.

tetraoxo polyhedron ($\Delta \simeq 11\,500 \pm 500$ cm^{-1}).[19] The B value is completely unreasonable and not correct, as will be shown below.

It is the intention of this paper to present a series of spectra that originate from tetrahedral Cr(IV) in various host compounds and to properly assign the bands. These assignments will be based on quantitative calculations of the term energies within the "angular overlap" model. Here the geometries of the host tetrahedra serve as input parameters. Analogous to the case of the isoelectronic Mn^{5+} ion in host tetrahedra of oxidic solids, zero-field splitting effects in the EPR spectra due to low-symmetry ligand field components[19b] and interesting luminescence properties[20] are expected. Luminescence transitions are indeed observed[21a] and will be the subject of a separate contribution.[21b]

The tendency of Cr^{4+} to disproportionate into Cr^{3+} and Cr^{5+} is the major difficulty in preparing pure Cr(IV)-containing solids. This tendency is particularly pronounced in melts and has prevented so far the synthesis of pure Cr(IV)-doped single crystals—the exception being γ-Ca_2GeO_4 (Cr(IV)) (see below).

In the first series of experiments, we used compounds with GeO_4 host tetrahedra, because Ge^{4+} (0.38 Å^4) has an ionic radius comparable to that of Cr^{4+} and also possesses a similar $3d^n$ electronic configuration. The chosen host structures for the isomorphic substitution are $M^{II}_2GeO_4$ [M^{II}: Ca, Sr, Ba], Ba_3GeO_5, and $Ba_2ZnGe_2O_7$ (Table 1). Secondly, Cr^{4+} was generated in situ from Cr^{5+}-containing solids by various reduction procedures. In particular, we used the compounds $Ca_2(PO_4)_{1-x}(CrO_4)_xCl$ and $Ca_5(PO_4)_5(CrO_4)_{5-x}Cl(Br)$, with spodiosite and apatite structures, respectively, as initial materials. A treatment under reducing conditions (or by X-ray irradiation) leads to compounds that partly or predominantly contain Cr^{4+} (see Experimental Section)—presumably formed by the generation of vacancies on the Cl^- (Br^-) positions.

Experimental Section

Synthesis and Characterization. Olivine-type[22] mixed crystals $Ca_2Ge_{1-x}Cr_xO_4$ were prepared by the solid state reaction of $CaCO_3$, GeO_2, Cr_2O_3, and CrO_3 in the appropriate molar amounts at 1250 °C in a corundum boat and under flowing argon (heating period 10 h). After thorough homogenization in a mortar, a second sintering procedure under the same conditions was applied. Turquoise-green powders were obtained, which were pure up to $x = 0.3$ as indicated by the X-ray Guinier technique. The oxidation state of chromium (iodometric analysis) was 4.0 ± 0.1.

Mixed crystals $Ba_2Ge_{1-x}Cr_xO_4$ could be prepared by applying the same experimental conditions as described below for the Sr^{2+} compounds. The samples were homogeneous and pure only up to $x < 0.1$, however, and appeared green. At higher x values $Ba_3(CrO_4)_2$ appears as an impurity phase. The lattice parameters of the Cr(IV)-doped solids are close to those of Ba_2GeO_4 ($a = 5.985$ Å, $b = 7.585$ Å, $c = 10.430$ Å; presumable space group *Pnma*[23]), while Ba_2CrO_4—which we were not able to synthesize in a pure state—is reported to possess unit cell dimensions $a = 5.914$ Å, $b = 7.629$ Å, and $c = 10.464$ Å (space group *Pnma*, No. 62).[6] We have based our AOM calculations on the data in ref 6 rather than on those in ref 5, which imply a different space group ($Pna2_1$) and also slightly different lattice constants ($a = 7.67$ Å, $b = 5.89$ Å, $c = 10.39$ Å), because the reported average Cr−O spacings of 1.75_5 Å (1.81_5 Å^5) nicely match with those in other oxidic Cr(IV) compounds.

The complete mixed-crystal series $Sr_2Ge_{1-x}Cr_xO_4$ could be synthesized from $Sr(OH)_2$, $SrCrO_4$, Cr_2O_3, and GeO_2 by following the experimental procedure proposed by Scholder[24] (three sintering periods

(19) (a) Reinen, D.; Lachwa, H.; Allmann, R. *Z. Anorg. Allg. Chem.* **1986**, *542*, 71. (b) Lachwa, H.; Reinen, D. *Inorg. Chem.* **1989**, *28*, 1044.
(20) (a) Herren, M.; Güdel, H. U.; Albrecht, C.; Reinen, D. *Chem. Phys. Lett.* **1991**, *183*, 98. (b) Herren, M.; Riedener, T.; Güdel, H. U.; Albrecht, C.; Kaschuba, U.; Reinen, D. *J. Lumin.* **1992**, *53*, 452. (c) Oetliker, U.; Herren, M.; Güdel, H. U.; Kesper, U.; Albrecht, C.; Reinen, D. *J. Chem. Phys.* **1994**, *100*, 8656.
(21) (a) Brunold, Th.; Herren, M.; Oetliker, U.; Güdel, H. U.; Kesper, U.; Albrecht, C.; Reinen, D. *J. Lumin.* **1994**, *60/61*, 138. (b) Oetliker, U.; Hazenkamp, M. F.; Güdel, H. U.; Atanasov, M.; Kesper, U.; Reinen, D. To be published.
(22) Shigekazu, U.; Kazuyori, U.; Keiichi, K. *Semento Gijetsu Nenpo* **1975**, *29*, 32.
(23) ASTM data base 39-1257 (1992).
(24) Scholder, R.; Sperka, G. *Z. Anorg. Allg. Chem.* **1956**, *51*, 285.

at 900 °C for 4 h each time). Heating under flowing nitrogen produced partly Cr(V) compounds, such as the $Sr_5(CrO_4)_3OH$ apatite, however, and only treatment under a vacuum of 10^{-5} Torr yielded pure compounds, which were turquoise blue at low and dark greenish blue at high Cr(IV) concentrations. From the powder X-ray diagrams we deduce that Sr_2GeO_4 probably crystallizes in a β-K_2SO_4-type structure with unit cell parameters $a = 7.05(2)$ Å, $b = 5.77(1)$ Å, and $c = 10.14$-(1) Å. They compare well with those reported for Sr_2CrO_4 ($a = 14.182$ Å, $b = 5.788$ Å, $c = 10.100$ Å; space group $Pna2_1$, No. 33[7]). Apparently there is only one tetrahedral position, however, because the a constant is only half of that for Sr_2CrO_4. It should be noted that the X-ray reflection intensities reported for Sr_2CrO_4 (single-crystal analysis[7]) differed markedly from those observed by us for powder samples.

Compounds $Ba_2MgGe_{2-x}Cr_xO_7$ with the Akermanit structure[25] were synthesized by heating Ba_2CO_3, MgO, GeO_2, Cr_2O_3, and CrO_3 at 800 °C under argon for 12 h and subsequently, after homogenization, a second time at 1000 °C under flowing argon (12 h). Only a few molar percents can be isomorphously incorporated into the lattice, and always $BaCrO_4$ is present as the second phase. The mixed crystals possess green colors.

Mixed crystals $Ba_3Ge_{1-x}Cr_xO_5$ were prepared from homogeneously mortared mixtures of $BaCrO_4$, Cr_2O_3, GeO_2, and $Ba(OH)_2{\cdot}8H_2O$ in the respective molar amounts, but with the latter compound in excess. The reactive powder was dehydrated at about 150 °C, mortared again, and slowly heated in an evacuated quartz tube ($<10^{-1}$ bar) to 1000 °C and kept at this temperature for 10 h. The compounds contained BaO impurities, which had no influence on the spectroscopic properties. The host lattice Ba_3GeO_5 possesses the same Cs_3CoCl_5 structure as Ba_3CrO_5 and presumably also the space group $I4/mcm$[26] (Table 1). The complete mixed-crystal series could be synthesized, with the unit cell parameters changing from $a = 7.34_3$ Å, $c = 11.58_{(5)}$ Å ($x = 0$) to $a = 7.30_2$ Å, $c = 11.69_{(5)}$ Å ($x = 1.0$) [Guinier values] in a linear fashion.

We were able to stabilize Cr(IV) in the apatite structure (see Table 1) by preparing the Cr(V) compounds first and imposing reducing sintering procedures in a second step. The apatite phases $Ca_5(PO_4)_{3-x}(CrO_4)_xCl[Br]$ were synthesized from P_2O_5, $CaCrO_4$, Cr_2O_3, and $CaCl_2[Br_2]$ in the respective molar ratios. After a heating period of 3 h at 400 °C under flowing argon, the mixture was sintered at 900 °C during 12 h under argon atmosphere (stationary). The latter procedure was repeated after thorough homogenization by mortaring. The subsequent treatment at 900 °C for 7 h under a vacuum of $\simeq 10^{-3}$ bar transformed the pure green Cr(V) compounds into such containing predominantly or at least significantly Cr(IV) as indicated by the ligand field spectra (see Figure 8) and the color shift to bluish green or turquoise. The change in stoichiometry is accompanied by a distinct increase in the hexagonal unit cell parameters. We think that Cr(V) is reduced to Cr(IV) by the Cl^- [Br^-] anions, thus creating vacancies on the halide positions of the apatite lattice. This concept is supported by the observation that hydroxide apatites do not show this reductive behavior and that bromide apatites are more effective in generating Cr(IV) than those with chloride on the anionic positions.

Instead of applying vacuum to the Cr(V) cmpounds, we have also performed reduction reactions with sodium, according to

$$Ca_5(PO_4)_{3-x}(Cr^{V}O_4)_xCl + x\mathrm{Na} \rightarrow Ca_5(PO_4)_{3-x}(Cr^{IV}O_4)_xCl_{1-x}\square_x + x\mathrm{NaCl}$$

The reaction was performed in an evacuated sealed quartz capsule with a slight excess of sodium (30 h, 500 °C). Though we succeeded in to generating Cr(IV), a significant fraction always remained as Cr(V)—as was deduced from the iodometric analysis and the ligand field spectra.

We were also able to transform Cr(V) in the Cr(V) apatites partly into Cr(IV) by exposing the compounds to X-ray radiation for a few hours.

In all cases, the relative fraction of Cr(IV) became smaller with increasing total chromium content x.

Attempts to reduce chromium in spodiosite-type chromium(V) compounds $Ca_2(PO_4)Cl$ (Table 1) by vacuum treatment failed. A reduction was possible with sodium, presumably generating vacancies on the chloride positions again. The synthesis conditions were analogous to those applied for the apatite compounds. The turquoise color of the Cr(V) spodiosites changed to green or bluish green upon reduction. The iodometric analysis indicated only a minor chromium fraction to be still in oxidation state +V.

The purity of all samples was controlled by X-ray powder methods [diffractometry and Guinier technique], and the lattice constants were determined by using the same techniques.

Angular Overlap Calculations. Term energies and **g** tensor components were calculated within the angular overlap model (AOM) using the computer program AOMX developed by Adamsky.[30] In the AOM calculations we used the exact site geometries as given by the structural data. Reference values of e_σ and e_π, the parameters of σ- and π-antibonding, characterizing the Cr^{4+}–O bond are based on the best fit values from the absorption spectrum of Cr^{4+} doped into Ca_2GeO_4, valid for Cr–O spacings of $\simeq 1.77$ Å. Bond length variations and their influence on the Cr–O bonding parameters are approximated by overlap integrals using the relation

$$e_\lambda/e_\lambda' = S_\lambda^2/S_\lambda'^2 \qquad (\lambda = \sigma, \pi) \tag{1}$$

Overlap integrals are calculated by applying a program of Calzaferri and Brändle,[31] which uses double-ζ functions for Cr^{4+}, Cr^{5+}, and Cr^{3+} [32] and Slater functions for oxygen 2p orbitals.

More detailed information concerning the calculation procedure is given below.

Physical Methods. Powder reflectance spectra were recorded between 4000 and 50 000 cm^{-1} by a Zeiss PMQII and a Hitachi U-3410 spectrophotometer. The 5 K spectra were taken using a low-temperature attachment to the former instrument. The intensity scale is either the percentage of reflectance or $\log(k/s)$, as calculated from the diffuse reflectance using the theory of Kubelka-Munk.

X- and Q-band EPR measurements between 4 and 295 K were performed with a Bruker spectrometer, the exact microwave energy measured by a frequency meter.

Results and Discussion

d^2-configurated cations in T_d coordination are expected to induce three spin-allowed d–d transitions $^2A_2 \rightarrow {}^3T_2, {}_a{}^3T_1, {}_b{}^3T_1$, from which the first is symmetry-forbidden and the last one corresponds to a (nearly) two-electron jump and should also have a low intensity. Indeed, the ligand field spectra of tetrahedrally coordinated Mn^{5+} ions in various oxidic host lattices exhibit these features with only one intense band, which may be split by low-symmetry site distortions.[19,33] From the spin-forbidden transitions only those corresponding to $^3A_2 \rightarrow {}^1E, {}^1A_1$ are frequently seen as sharp features around 8600 and 13 300 cm^{-1}. The former is also observed in emission and has promising laser properties in some host structures.[21] Reported ligand field parameters are $\Delta = 11\,500 \pm 500$ cm^{-1}, $B \simeq 500$ cm^{-1}, and $C/B \simeq 4.0$. A more sophisticated procedure to fit published single-crystal and powder spectra within the AOM

(25) Allik, T. H.; Ferry, M. J.; Reeves, R. J.; Powell, R. C.; Hovis, W. W.; Caffey, D. P.; Utano, R. A.; Merkle, L.; Campana, C. F. *J. Opt. Soc. Am.* **1990**, *B7*, 1190.
(26) Mansmann, M. *Z. Anorg. Allg. Chem.* **1965**, *339*, 52.
(27) Mackie, P. E.; Elliott, J. C.; Young, R. A. *Acta Crystallogr.* **1972**, *B28*, 1840.
(28) (a) Greenblatt, M.; Banks, E.; Post, B. *Acta Crystallogr.* **1967**, *23*, 166. (b) Greenblatt, M.; Banks, E.; Post, B. *Acta Crystallogr.* **1969**, *B25*, 2170.
(29) Banks, E.; Greenblatt, M.; Post, B. *Inorg. Chem.* **1970**, *9*, 2259.
(30) Adamsky, H. *AOMX: A Fortran computer package*; Institut Theoretische Chemie, Heinrich-Heine-Universität: 40225 Düsseldorf, Germany.
(31) Calzaferri, G.; Brändle, M. Extended Hückel Calculations, ICONC & INPUTC. *QCPE Bull.* **1992**, *12*, No. 4.
(32) Richardson, J. W.; Nieuwport, W. C.; Powell, R. R.; Edgel, W. F. *J. Chem. Phys.* **1962**, *36*, 1057.
(33) (a) Borromei, R.; Oleari, L.; Day, P. *J. Chem. Soc., Faraday Trans.* **1977**, *73*, 135; **1981**, *77*, 1563. (b) Milstein, J.; Holt, S. L. *Inorg. Chem.* **1969**, *8*, 1021.

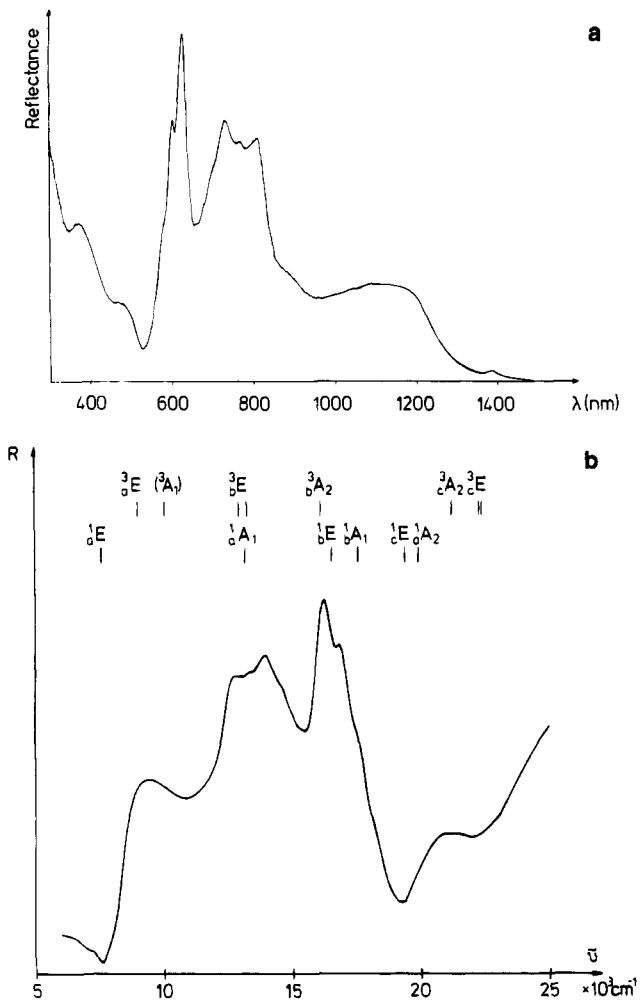

Figure 1. Powder reflectance spectra (298 K, arbitrary intensity scale) of Cr^{4+}-doped γ-Ca_2GeO_4 between 320 and 1500 nm (a) and in the visible region (b). The band assignment in C_{3v} symmetry and the transition energies derived from an AOM calculation (Table 2) on the basis of the host site GeO_4 geometry (Table 1) are given in the latter case. (The tiny irregularities at ≃7200 (and 5200) cm^{-1} are due to traces of OH^- or H_2O in the "white standard" of the reflectance measurement—see also Figures 3 and 5−10.)

approach suggests even lower B values around 400 cm^{-1}.[34] The latter B value implies a nephelauxetic ratio β of about 0.35 (B_0 = 1160 cm^{-1}, C_0/B_0 = 4.2$_5$, and ζ = 480 cm^{-1} are deduced from the free ion term diagram[35]).

Cr^{4+} in Ca_2GeO_4. An isomorphic substitution of Ge^{4+} by Cr^{4+} is possible up to 30 mol % with a small increase of the unit cell parameters, which is due to the somewhat larger ionic radius of Cr^{4+} compared to Ge^{4+} (see below). The ligand field spectrum exhibits the expected features with strong split bands between 12 500 and 17 000 cm^{-1} and weaker absorptions around 9500 and 21 000 cm^{-1}, which can be assigned to the $^3A_2 \rightarrow {}_a{}^3T_1$, $\rightarrow {}^3T_2$, and $\rightarrow {}_b{}^3T_1$ transitions in T_d symmetry, respectively (Figure 1). It does not change significantly with concentration and temperature and is already nicely resolved at 298 K.

A complete assignment on the basis of the qualitative arguments given above and an AOM calculation was possible. e_σ, e_π, and B were chosen as free variables, while the angular geometry of the GeO_4 host polyhedra—the site symmetry is C_s (Table 1), but very close to a trigonally elongated tetrahedron (C_{3v})—and the C/B ratio were used as fixed input parameters. The latter ratio was assumed to have the value of the free Cr^{4+} ion (B_0 = 1015 cm^{-1}, C_0/B_0 = 4.2, and ζ_0 = 330 cm^{-1}, derived from the Grotrian diagrams).[35,36] This assumption is well justified for oxidic compounds of low-valent d^n cations such as Ni^{2+} and Co^{2+} with a rather ionic metal to ligand bond,[38] meaning that B and C are depressed by the ligand field to the same extent. It turned out that the calculated energies are rather insensitive with respect to e_σ and e_π, so long as the ligand field parameter $\Delta = {}^4/_9(3e_\sigma - 4e_\pi)$ remained unchanged. Apparently the geometric deviation of the CrO_4^{4-} polyhedra from T_d symmetry is not large enough to induce anisotropic bonding properties such that e_σ and e_π can be determined separately without restrictions with respect to Δ. A very satisfactory fit for most observed transitions is achieved with Δ = 9620 cm^{-1} and B = 480 cm^{-1} (Table 2), with an arbitrary e_σ/e_π choice of about 6. The chosen C/B ratio reproduces quite well the positions of the $^2A_2 \rightarrow {}_a{}^1T_2$, transitions, while the calculated energies of the $^3A_2 \rightarrow {}_a{}^1E$, $^1A_1$ transitions (Table 2) are too low by about 10% with respect to the experimental values. The origin is most probably a different nephelauxetic effect for the configurations e^2, $e^1t_2^1$, and t_2^2, respectively, which was first proposed by Jorgensen ("symmetry-restricted covalency")[39] and which is clearly present in cases of larger ligand fields, such as oxidic Cr^{3+} compounds.[40] Because the $_a{}^1E$, $^1A_1$ terms originate from the same e^2 configuration as the $^3A_2$ ground state, reflecting only π-antibonding properties, the B_{ee} value is indeed expected to be larger than B_{et}. Having in mind that the two mentioned terms do not depend on Δ in the strong-field approximation, we estimate—with $C_{ee}/B_{ee} = 4.2$—B_{ee} to be about 530 cm^{-1}. Because all other terms with the exception of $_b{}^3T_1$ refer essentially (strong-field approximation) to the $e^1t_2^1$ configuration,

Table 2. Observed and Calculated Band Energies of Cr^{4+}-Doped Ca_2GeO_4 [in 1000 cm^{-1}; Δ = 9620 cm^{-1} (e_σ = 9320 cm^{-1}, e_π = 1580 cm^{-1}), B = 480 cm^{-1}, C/B = 4.2; Ground State $_a{}^3A_2$][a]

assignment			
T_d	C_{3v}	calcd	exptl
$_a{}^1E$	$_a{}^1E$	7.61	8.35[d]
$^3T_2$	$_a{}^3E$	8.99, 9.00	9.40
	$^3A_1$[b]	10.05	
$_a{}^3T_1$	$_b{}^3E$	12.96, 13.29	12.70, 13.15, 13.95
	$_b{}^3A_2$	16.21	16.20
$_a{}^1A_1$	$_a{}^1A_1$	12.99	≈14.50
$_a{}^1T_2$	$_b{}^1E$	16.50, 16.57	16.75
	$_b{}^1A_1$	17.57	≈17.50
$^1T_1$	$_c{}^1E$	19.36, 19.40	
	$^1A_2$	19.90	
$_b{}^3T_1$	$_c{}^3A_2$[c]	21.16	≈21.20
	$_c{}^3E$[c]	22.27, 22.40	

[a] The symmetry labeling is according to the approximately verified C_{3v} symmetry of the CrO_4^{4-} tetrahedra. LS coupling is not included (see text). [b] Symmetry-forbidden transition. [c] Weak transitions (approximately two-electron excitations). [d] In luminescence[21a] (see text).

(34) Atanasov, M.; Adamsky, H.; Reinen, D. Submitted for publication in *J. Chem. Phys.*
(35) Bashkin, S.; Stoner, J. O., Jr. *Atomic Energy-Level and Grotrian Diagrams*; North-Holland Publishing Co.: Amsterdam, Oxford, New York, 1982; Vol. 3 (Cr), Vol. 4 (Mn).
(36) Using the Trees correction $\alpha L(L + 1)$ in order to account for interactions of the free ion terms resulting from d^2 with terms of the same symmetry, which originate from configurations outside d^2,[37] the parameter set B_0 = 1075 cm^{-1}, C_0/B_0 = 3.6$_5$, and α = 90 cm^{-1} is deduced. With these values the free ion terms can be reproduced within ±200 cm^{-1}. We will refer to the nonrefined parameter set, however, in order to avoid a nonjustified sophistication in regard to mostly rather broad optical transitions in the powder spectra.
(37) Griffith, J. S. *The theory of transition metal ions*; Cambridge University Press: Cambridge, U.K., 1971.
(38) Reinen, D. *Struct. Bonding* **1969**, *7*, 114 and cited references.
(39) Jorgensen, C. K. *Orbitals in atoms and molecules*; Academic Press: New York, 1962.
(40) Reinen, D. *Struct. Bonding* **1969**, *6*, 30.

the above best-fit B value of 480 cm^{-1} would correspond to a B_{et} notation. The $^3A_2 \rightarrow {}_b{}^3T_1$ transition corresponds to an excitation of (nearly) two electrons into the ($\sigma\oplus\pi$)-antibonding t_2 state and should induce an even lower B_{tt} parameter. Indeed, the calculated energies for the corresponding weak band are always too large with respect to the spectral observations (Figures 1, 3, 7, 8, and 10). In agreement with these considerations are the results of an ab-initio calculation for the $Cr(OH)_4$ model complex with reported B values of $B_{ee} = 565$ cm^{-1}, $B_{et} = 495$ cm^{-1}, and $B_{tt} = 425$ cm^{-1}.[41] They are slightly larger than those found for Cr^{4+}-doped Ca_2GeO_4, apparently due to the somewhat less pronounced nephelauxetic effect of "OH" compared to "O".

The comparison of the observed and calculated transition energies (Figure 1, Table 2)—bearing in mind that three different B values are present—is sufficiently good to serve as an additional convincing argument that the spectra originate from Cr^{4+} in tetrahedral coordination, and for the purity of the $Ca_2Ge_{1-x}Cr_xO_4$ mixed crystals as well. Further support comes from the 4.2 K single-crystal spectra, which will be reported and discussed separately.[21b] The luminescence properties also indicate only one chromium species and locate the ^1E state at 8350 cm^{-1}.[21a] Very probably, strong mixing with the lowest-energy split term of the $^3T_2$ state occurs, however. The $^3A_2 \rightarrow {}^1E$ transition is detected in the powder spectrum at 5 K as a weak shoulder at about 8.000 cm^{-1} in the low-frequency part of the $^3E(^3T_2)$ band as well. Surprisingly, it occurs at energies comparable to those of Mn(V)-doped oxidic solids[19,20,33] (see below).

Taking the slightly differing M−O spacings in the host tetrahedra into account, the additionally produced energy shifts do not exceed 200 cm^{-1} with respect to those given in Table 2. LS-coupling effects were neglected when the term energies in Table 2 were calculated because its influence is rather small (see below) and would obscure splittings due to low-symmetry ligand field components. Possibly the lower-symmetry component of the CrO_4^{3-} polyhedron is more distinct than that of the GeO_4^{3-} host tetrahedron. This is indicated by the observed rather pronounced splitting of the ${}_b{}^3E$ term compared to the calculation (Figure 1) and confirmed by the intensity distribution in the calculated spectrum.

In the proposed assignment it was assumed that the broad band at 26 500 cm^{-1} is not a d−d transition because its intensity is by far too high for the two-electron ${}_a{}^3A_2 \rightarrow {}_c{}^3E({}_b{}^3T_1)$ excitation, which would otherwise be expected to appear in this energy region (Table 2). Since the absorption spectrum of Ca_2GeO_4 does not show this transition, we can tentatively assign the broad band to a low-lying weak charge transfer transition of Cr(IV) or more probably to the charge transfer of $Cr(VI)O_4^{2-}$ polyhedra, present in traces of an impurity phase.

The ligand field parameter of 9600 cm^{-1} is reduced with respect to those of Mn(V) ($\simeq$11 500 ± 500 cm^{-1}) and Cr(V) ($\simeq$12 000 ± 500 cm^{-1} [42]) by about 20%—well in accord with the lower by one oxidation state. The nephelauxetic ratio β ($=B_{et}/B_0$) is 0.47 and substantially larger than the one for Mn^{5+} in similar host compounds[19,34] ($\beta \simeq 0.35$). Interestingly enough, a very low B value is also reported for the $Fe^{VI}O_4$ polyhedron,[43] with not only the ^1E but also the $^1A_1$ term (which both are nearly independent of Δ) appearing at energies lower than that of the first triplet−triplet transition. The estimated β value is distinctly lower than 0.3. The decreasing nephelauxetic ratios in the sequence Cr(IV), Mn(V), and Fe(VI) indicate the expected increasing covalency of the metal−ligand bond. The same trend is observed for the metal-to-ligand charge transfer bands,[19,43] which appear as low as 16 000 cm^{-1} in the case of Fe(VI),[43] reflecting the pronounced instability of the latter oxidation state.

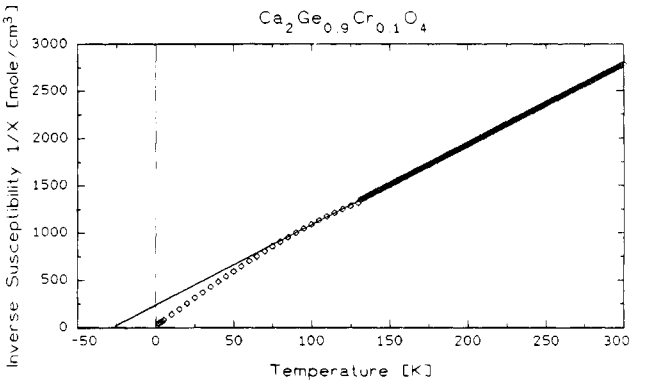

Figure 2. Inverse magnetic susceptibility versus temperature plot for Cr^{4+} in γ-Ca_2GeO_4 ($\mu_{Cr} = 3.0\ \mu_B$, $\Theta_p = -28$ K, applied field 30 kG).

The reported values of $B \simeq 860$ and 795 cm^{-1} for Cr^{4+}-doped forsterite[17] and $Cr(O^tBu)_4$,[2] respectively, are by far too great. The information presented in Table 2 fixes B to a much lower value, which is also consistent with those for the isoelectronic Mn^{5+} and Fe^{6+}, as just discussed.

The EPR spectra of mixed crystals $Ca_2Ge_{1-x}Cr_xO_4$ with very low Cr^{4+} content taken at low temperatures clearly exhibit zero-field-splitting effects. Though they are not too well resolved, a D parameter of 0.13(1) cm^{-1} could be deduced, while E is very small. The observed D value can be reproduced by the AOM calculations with a nearly isotropic g value of $\simeq$1.94 and a ζ parameter of 165 cm^{-1} [$E = 0.01_5$ cm^{-1}], corresponding to a reduction of ζ_0 by 50%, nicely matching with the nephelauxetic ratio. The given values are also consistent with the orbital contributions in eq 2. Magnetic susceptibility measurements on

$$g = g_0 - 4\zeta_{eff}/\Delta \qquad (2)$$

samples with Cr^{4+} concentrations between 0.1 and 0.3 yielded μ_{eff} values of 2.8 ± 0.2 μ_B, well in accord with the expected spin-only moment of chromium(IV). The reason for the significantly varying experimental moments is most probably an uncertainty with respect to the exact amount of Cr^{4+} incorporated into the GeO_4 host site due to the solid state synthesis. A typical $1/\chi_{mol}$ versus T plot is shown in Figure 2. The negative Θ_p value indicates weak antiferromagnetic spin−spin interactions.

Cr^{4+} in Ba_2GeO_4. Figure 3 exhibits a typical absorption spectrum of Cr^{4+} in the Ba_2GeO_4 host lattice, showing again the prominent feature of the symmetry-split $^3A_2 \rightarrow {}_a{}^3T_1$ transition together with weak maxima and shoulders due to the two other triplet−triplet transitions. The calculated transition energies, based on the C_s geometry of the CrO_4^{4-} polyhedra in Ba_2CrO_4 (Table 1), the reference AOM parameters of Cr^{4+} in Ca_2GeO_4 valid for a mean Cr−O spacing of 1.77 Å (Table 2), $B = 470$ cm^{-1} and $C/B = 4.2$, are indicated. The widely varying Cr−O spacings in Ba_2CrO_4 were explicitly taken into account, but adjusted to yielding a mean distance of 1.77 Å. The agreement between observed and calculated transition energies is sufficiently good to be certain in this case also that the spectrum is the one of Cr^{4+} in the GeO_4^{4-} host polyhedra of Ba_2GeO_4. It is indeed not expected that the geometry of Cr^{4+} on the GeO_4 site in Ba_2GeO_4 is *exactly* the one of CrO_4^{4-} in Ba_2CrO_4. Bearing in mind that the ^1E term was observed at an about 800

(41) Atanasov, M.; Adamsky, H.; Eifert, K. To be published.
(42) Reinen, D.; Albrecht, C.; Kaschuba, U. *Z. Anorg. Allg. Chem.* **1990**, *584*, 71.
(43) (a) Herren, M.; Güdel, H. U. *Inorg. Chem.* **1992**, *31*, 3683. (b) Brunold, Th.; Hauser, A.; Güdel, H. U. *J. Lumin.* **1994**, *59*, 321.

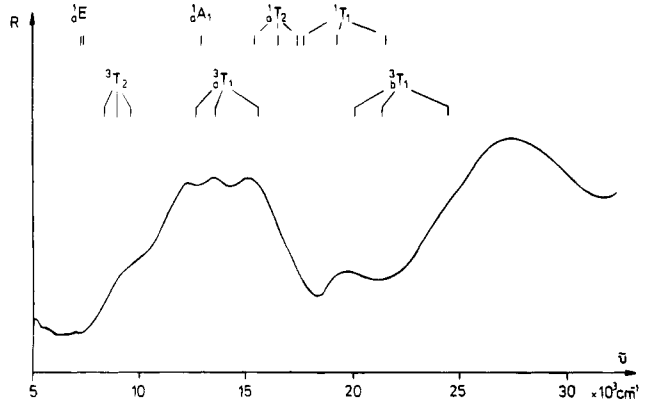

Figure 3. Powder reflectance spectrum (298 K, arbitrary intensity scale) of Cr^{4+} in Ba_2GeO_4. The given energies are those calculated in the AOM on the basis of the CrO_4^{4-} geometry (C_s) in Ba_2CrO_4, with e_σ and e_π values as in Table 2 and $B = 470$ cm^{-1} (see text). The tetrahedral parent terms are indicated.

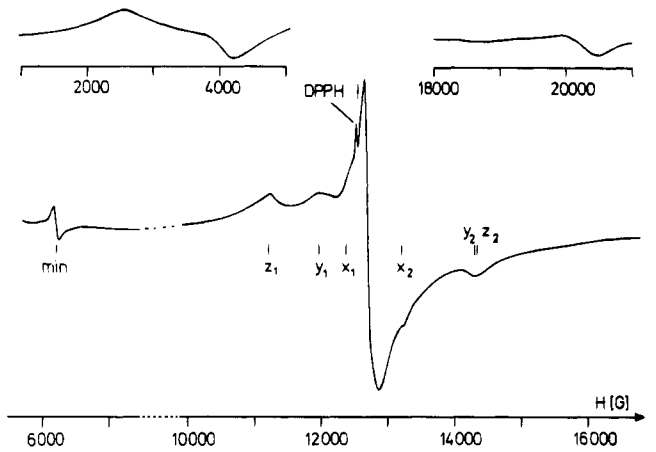

Figure 4. Q-Band EPR spectrum of Cr^{4+}-doped Ba_2GeO_4. The indicated positions are those corresponding to $D \simeq 0.14$ cm^{-1}, $E \simeq 0.025$ cm^{-1}, and g values between 1.92 and 1.95 (see text). The additional features at very high and low fields indicate a second center with considerably larger fine structure components.

cm^{-1} higher energy compared to the calculated value in the case of Cr(IV) in Ca_2GeO_4 (see preceding section), it is here expected to appear even closer to the lowest split term of $^3T_2$. This may again lead to interesting luminescence properties.[21]

Though the powder EPR spectra are predominantly determined by a central signal at $g_{eff} = 1.98$, features due to a spin–triplet zero-field splitting are clearly resolved, including the half-field signal (Figure 4). It is possible to nicely reproduce the positions of the Q-band fine structure signals between 6000 and 15 000 G with $D \simeq 0.14$ cm^{-1}, $E \simeq 0.025$ cm^{-1}, and g values varying between 1.91 and 1.95. Additional features are observed at very large and very low magnetic fields, indicative of a second species with considerably larger zero-field splitting. The calculated zero-field splitting on the basis of the CrO_4 geometry in Ba_2CrO_4 (Table 1, Figure 4) yields—with $\zeta = 165$ cm^{-1}—$D = 1.00$ cm^{-1} and $E = 0.15$ cm^{-1} ($g_{xy} \simeq 1.92$, $g_z \simeq 1.95$). These values presumably correlate with the second center. We may suggest that two sites in Ba_2GeO_4 with rather different extents of distortion are present.

The Mixed-Crystal Series $Sr_2Ge_{1-x}Cr_xO_4$. The powder reflectance spectra of mixed crystals $Sr_2Ge_{1-x}Cr_xO_4$ (Figure 5) are roughly similar to those observed for Cr^{4+}-doped γ-Ca_2GeO_4 and Ba_2GeO_4. The intensity-dominating $^3A_2 \rightarrow {}_a{}^3T_1$ transition—with split bands around 12 500, 14 500, and 16 000 cm^{-1}, which are fully resolved at 5 K—and the weak $^3A_2 \rightarrow {}^3T_2$ (shoulder at ≃9500 cm^{-1}) and $\rightarrow {}_b{}^3T_1$ (≃20 500 cm^{-1})

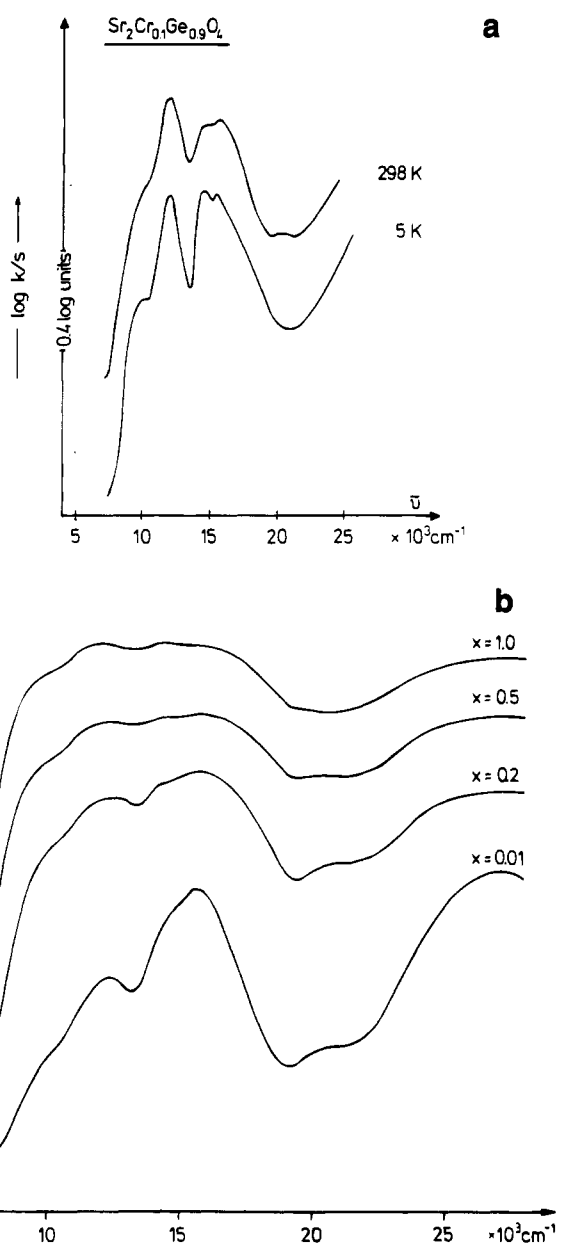

Figure 5. Powder reflectance spectra of $Sr_2Ge_{1-x}Cr_xO_4$ mixed crystals: $x = 0.1$ at 298 and 5 K (a); $0.01 \leq x \leq 1.0$ at 298 K (reflectance in arbitrary scale) (b).

transitions clearly indicate the presence of CrO_4^{4-} tetrahedra. There is no significant shift in the energy positions of the absorption bands with increasing x, though the relative intensity distribution changes, with the peak around 16 000 cm^{-1} becoming less prominent at higher x values (Figure 5b). We were not able to find any sufficiently good correlation between the transition energies in the spectrum and the energies calculated by the AOM on the basis of the two independent CrO_4^{4-} sites in Sr_2CrO_4.

In the EPR spectra only one signal at $g_{eff} = 1.97$ is detected, even at low x values. Apparently it represents again the exchange average over a zero-field-splitting spectrum, implying that the isomorphous incorporation of Cr^{4+} into the GeO_4^{4-} sites occurs in clusters.

The discrepancy between the ligand field spectra of Sr_2CrO_4 *powder* samples and the site geometries of the mentioned CrO_4^{4-} polyhedra in Sr_2CrO_4, as elucidated by *single-crystal* X-ray analysis, may give rise to the speculation as to whether the two sites in Sr_2CrO_4 single crystals are due to $Cr^{III}O_4^{5-}$ and $Cr^{V}O_4^{3-}$

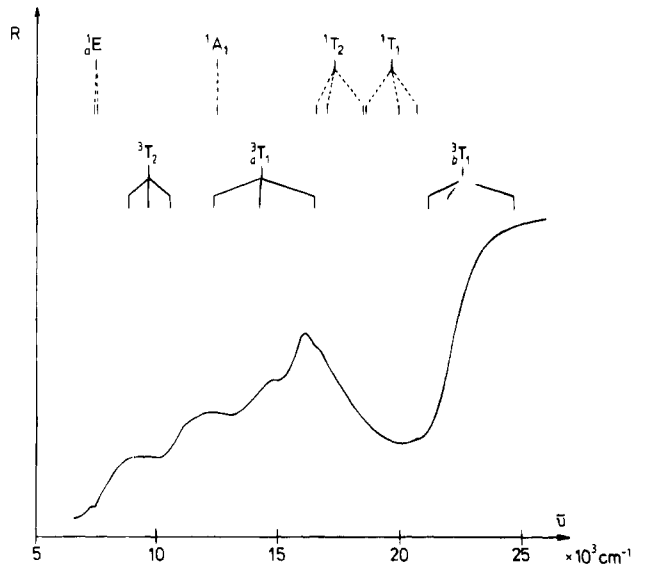

Figure 6. Powder reflectance spectrum (298 K, arbitrary intensity scale) of Cr^{4+}-doped $Ba_2MgGe_2O_7$. The assignment and the calculated energy positions originate from AOM calculations (Table 2) on the basis of the host site GeO_4 geometry (C_s) with by about 0.02 Å enhanced bond lengths (see text). The T_d parent terms are also indicated.

polyhedra. As mentioned in the Experimental Section, Cr(IV) has indeed a strong tendency in melts to disproportionate into Cr(III) and Cr(V). In support of this suggestion, site 2 with the longer Cr−O spacings, which would have to be assigned to Cr(III), exhibits an unusually large angular distortion, corresponding approximately to a trigonal compression. This is exactly the sign of distortion expected for tetrahedral Cr^{3+} as induced by vibronic Jahn−Teller coupling, generating a $_a{}^4A_1$ split term as the new ground state from the $_a{}^4T_1$ parent ground state.

Cr^{4+} in $Ba_2MgGe_2O_7$. The angular distortion of the GeO_4 polyhedra in akermanite roughly corresponds to a trigonal elongation as in Ca_2GeO_4, but in a more pronounced way and with a much larger lower-symmetry distortion component (C_s site symmetry; Table 1). A substitution of Ge^{4+} by Cr^{4+} was possible up to only a few mole percent. In the ligand field spectrum (Figure 6) four prominent absorption maxima at about 9500, 12 500, 14 500, and 16 200 cm^{-1} are observed. In order to assign the spectra, we again performed angular overlap calculations using the geometry of the Ge^{4+} site (Table 1) and the parameter set of Table 2, but with the Cr−O spacings adjusted to yield an average distance of 1.79 Å. With these larger by 0.02 Å spacings, a rather good agreement between calculated and observed band positions was achieved (Figure 6). On the basis of these results, we assign the broad band at ≈9500 cm^{-1} to the lowest two split components of $^3T_2$ and the band maxima at 12 500, 14 500, and 16 200 cm^{-1} to the $^3A_2 \rightarrow {}_a{}^3T_1$ transition. The considerable lower symmetry ligand field component leads to significant mixing of the $_a{}^3T_1$ and $_b{}^3T_1$ split terms and to a shift of the $^3A_2 \rightarrow {}_b{}^3T_1$ transitions to higher energies (21 000−24 600 cm^{-1}). They are hidden under the broad and unresolved absorption band centered at 26 000 cm^{-1}, which is a charge transfer band due to CrO_4^{2-}. As mentioned in the Experimental Section, $BaCrO_4$ is always present as an impurity phase.

The zero-field-splitting parameters D and E have been also calculated. Adopting a value of ζ = 165 cm^{-1} as in Cr^{4+}-doped Ca_2GeO_4, we obtain D = 1.16 cm^{-1} and E = 0.13 cm^{-1}. While the E value nicely matches with the one recently deduced (E = 0.15 cm^{-1}) from single-crystal EPR data,[15] the reported

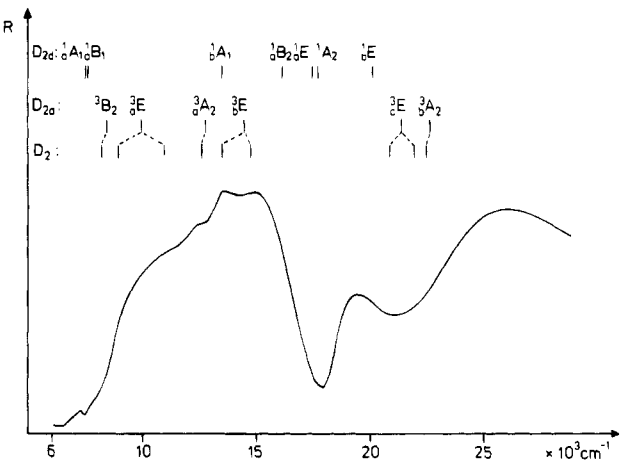

Figure 7. Diffuse reflectance spectrum (298 K, arbitrary intensity scale) of Cr^{4+}-doped Ba_3GeO_5 (1 mol %). The band assignment is based on AOM calculations with the parameter set of Table 2. The angular geometry is compressed D_{2d} (as in Ba_3CrO_5, Table 1) and (for the triplet−triplet transitions) modified to D_2 by an additional orthorhombic component (see text).

value of D = 3.80 cm^{-1} is much larger compared to our calculations. It would correspond to a LS-coupling constant $\zeta \simeq 0.9\zeta_0$ and seems to be unrealistically high. Also the reported g values (g_x = 1.99, g_y = 1.89, g_z = 2.00; $\bar{g} \simeq$ 1.96) differ significantly from those deduced from our calculations (1.93_5, 1.92, 1.95).

We conclude that the optical data and EPR spectra serve as a good test for the geometry of Cr^{4+} at the GeO_4 sites in akermanite as well. The available data and their analysis on the basis of our AOM calculations indicate that Cr^{4+} adopts—as in Ca_2GeO_4 and Ba_2GeO_4—largely the geometry of the GeO_4^{4-} host site, with a small adjustment of the bond distances.

The Mixed-Crystal Series $Ba_3Ge_{1-x}Cr_xO_5$. The powder reflectance spectra again show the typical features of a tetrahedral d^2 system (Figure 7) and do not change with increasing Cr^{4+} concentration. The $^3B_1(^3A_2) \rightarrow {}_a{}^1A_1, {}_a{}^1B_1({}_a{}^1E)$ transitions are detected as sharp peaks in the 5 K powder reflectance spectrum at ≃7800 and ≃8050 cm^{-1}. The $^3B_1(^3A_2) \rightarrow {}^3B_2(^3T_2)$ transition is symmetry forbidden in D_{2d}. In contrast to the compounds discussed so far, the site symmetry of Cr^{4+} is approximately tetragonal, as indicated by the Cs_3CoCl_5 structure of Ba_3CrO_5 (Table 1).

The observed band positions are reasonably well reproduced with the parameter set of Table 2 and an angle of elongation of 104.9° (Table 1). The fit is considerably improved by the assumption of a slightly more distinct tetragonal elongation and particularly the inclusion of a pronounced orthorhombic distortion component ($D_{2d} \rightarrow D_2$: 104.0°[2×], 108.8°[2×], 114.8°-[2×]—see Figure 7). It nicely reproduces the split peaks at 13 500 and 15 000 cm^{-1}. As discussed before, the triplet−singlet transitions within the e^2 configuration are calculated to occur at too low energies and the $^3B_1(^3A_2) \rightarrow {}_c{}^3E, {}_b{}^3A_2({}_b{}^3T_1)$ transitions at too high energies using a single B value of 480 cm^{-1}, as the consequence of symmetry-restricted covalency.

The EPR powder spectra exhibit an exchange-narrowed and nearly isotropic signal at $g_{eff} \simeq$ 1.99. Apparently—as in most investigated mixed crystals—the substitution of Ge^{4+} by Cr^{4+} occurs in clusters.

Cr^{4+} in Apatite-Type Phases. The powder reflectance spectrum in Figure 8 is due to CrO_4^{4-} polyhedra in $Ca_5(PO_4)_{2.97}(CrO_4)_{0.03}Br_{1-x}$ ($x < 0.03$), but superimposed by spectral features of tetrahedral Cr(V)—as is evident by comparison with

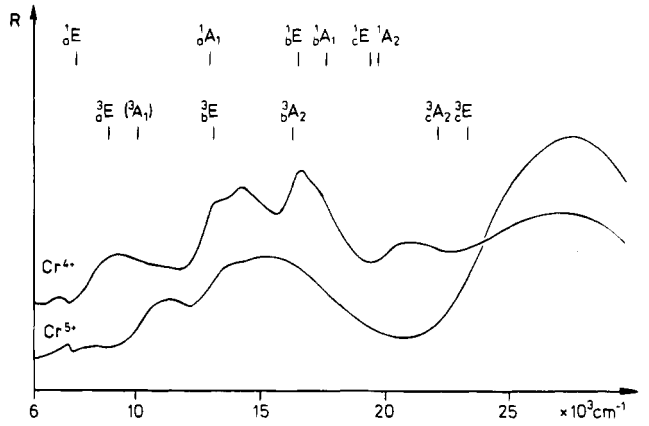

Figure 8. Diffuse reflectance spectrum (298 K, arbitrary intensity scale) of $Ca_5(PO_4)_{2.97}(CrO_4)_{0.03}Br_{1-x}$ ($x < 0.03$) in comparison with that of $Ca_5(PO_4)_{2.5}(CrO_4)_{0.5}Cl$. The band assignment of the former spectrum was based on an AOM calculation with the parameter set of Table 2 and a C_{3v} geometry (trigonal elongation 116°).

the spectrum of $Ca_5(PO_4)_{2.5}(CrO_4)_{0.5}Cl$ possessing absorption bands at 11 500, 13 500, and 15 500 cm^{-1}.[44] The first Cr(V) transition is weakly indicated in the bromide apatite spectrum, while the second may contribute to the intensity of the absorption at 13 200 cm^{-1}. The third one finally rises the minimum around 15 500 cm^{-1} (see below). With these features in mind, the bromide spectrum looks surprisingly similar to the that of Cr^{4+}-doped γ-Ca_2GeO_4 (Figure 1). This is indeed expected because the PO_4^{3-} and GeO_4^{4-} host sites are both trigonally elongated (C_{3v}), with a lower-symmetry component superimposed, leading to a C_s site symmetry in both cases (Table 1). The extent of the tetrahedron distortion in the apatite lattice increases if P(V) is substituted by larger cations. This can be shown spectroscopically when Mn(V) and Cr(V) substitute P(V),[19b,34,44] and is also in accord with the structural data for $Sr_5(CrO_4)_3Cl$ and $Ca_5(CrO_4)_3OH$. In these compounds the three larger O1–Cr–O2(O3) angles are 114.7 and 114.1° on the average, respectively, distinctly larger than the corresponding O–P–O angles in $Ca_5(PO_4)_3Cl$ (≈111.7°, Table 1) and approaching those of GeO_4^{4-} in γ-Ca_2GeO_4 (115.7°). Besides this argument, it is not necessarily expected that the geometry of the CrO_4^{4-} polyhedra in the investigated apatite compounds will follow exactly the one of the CrO_4^{3-} entities in the same structure because Cr(IV) is even larger and more polarizable than Cr(V).

A model calculation in C_{3v} with trigonal angles of 116° and the parameter set of Table 2 reproduces the main features of the spectrum (Figure 8), indicating that the host lattice still strongly determines also the geometry of the CrO_4^{4-} guest tetrahedra. The splitting of the $_b{}^3E(_a{}^3T_1)$ state into peaks at 14 300 and 13 200 cm^{-1} is in agreement with the expected presence of a lower-symmetry distortion component (Table 1).

The spectra collected in Figure 9 exhibit the same features as those discussed above, though different experimental techniques were applied to generate CrO_4^{4-} polyhedra in the apatite lattice (see Experimental Section). An increase of the relative Cr(V) content is nicely mirrored not only by the respective d–d transitions becoming more evident but also by a considerable intensity increase of the charge transfer band at 27 500 cm^{-1}. EPR spectra of some compounds were indicative of tetrahedral Cr(IV) with an exchange-averaged signal at about 1.955(5), superimposed by the anisotropic spectrum due to CrO_4^{3-}

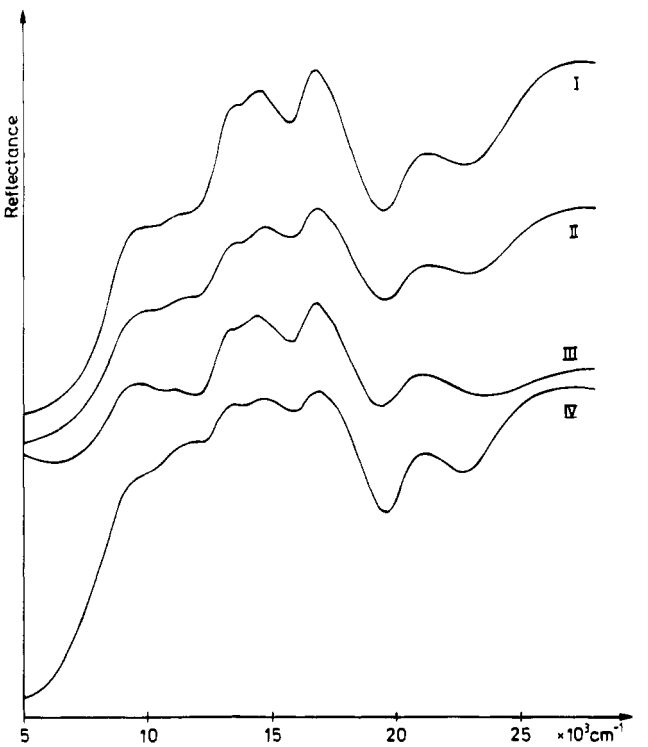

Figure 9. Diffuse reflectance spectrum (298 K, arbitrary intensity scale) of tetrahedral Cr(IV) in apatite-type compounds, with Cr(V) absorption features superimposed: (I, II) $Ca_5(PO_4)_{2.9}(CrO_4)_{0.1}Cl_{1-x}$ ($x < 0.1$)—sintered in vacuum and after X-ray radiation treatment, respectively; (III) $Ca_5(PO_4)_{2.9}(CrO_4)_{0.1}Br_{1-x}$ ($x < 0.1$); (IV) $Ca_5(PO_4)_{2.75}(CrO_4)_{0.25}Cl_{1-x}$ ($x < 0.25$)—reduction with sodium.

polyhedra.[42,44] A rough estimation of the zero-field splitting from the half-field signal H_{min} yielded $D \approx 0.45$ cm^{-1}.

Cr^{4+}-Doped Spodiosite-Type Compounds. The powder reflectance spectra of mixed crystals $Ca_2(PO_4)_{1-x}(CrO_4)_xO_4Cl_{1-y}$ with $y < x$ generated by the reduction of the corresponding Cr(V) spodiosites ($y = 0$) also exhibit the typical spectral features of a tetrahedral d^2 cation in comparison to Cr(V), namely the appearance of a distinct shoulder around 9500 cm^{-1} ($^3A_2 \rightarrow {}^3T_2$ transition) and of a weak absorption at ≈21 000 cm^{-1} ($^3A_2 \rightarrow {}_b{}^3T_2$, two-electron excitation) (Figure 10), hence strongly indicating the presence of Cr(IV). Distinct d–d absorption contributions due to Cr(V) cannot be detected anymore, as comparison with the spectrum of an unreduced Cr(V) spodiosite[44] clearly reveals (Figure 10). However, though the intensity of the first charge transfer band around 27 500 cm^{-1} has decreased considerably in intensity, it is still rather strong in comparison to that of Cr^{4+}-doped Ca_2GeO_4, for example (Figure 1), suggesting the presence of some Cr(V).

The host tetrahedra in spodiosite-type compounds are tetragonally distorted as in Ba_3CrO_5 (Table 1), but the sign of distortion is a compression rather than an elongation, with a small lower-symmetry component superimposed. Following the arguments in the preceding section, we have tried to estimate the energy positions of the Cr(IV) transitions using an AOM model calculation on the basis of a site that is tetragonally compressed with an angle of 118.5° and otherwise using the parameter set of Table 2. The fit is satisfactory for all observed spectral features besides the band at 16 500 cm^{-1}. Though there is a Cr(V) transition in this region ($^2A_1(^2E) \rightarrow {}^2B_2(^2T_2)$[44]), it is not expected to be as prominent as observed. Possibly the site geometry is rather different from the chosen one because—as discussed before—the CrO_4^{4-} tetrahedra may distort differently from the PO_4^{3-} host polyhedra.

(44) Albrecht, C.; Cohen, S.; Mayer, I.; Reinen, D. *J. Solid State Chem.* **1993**, *107*, 218.

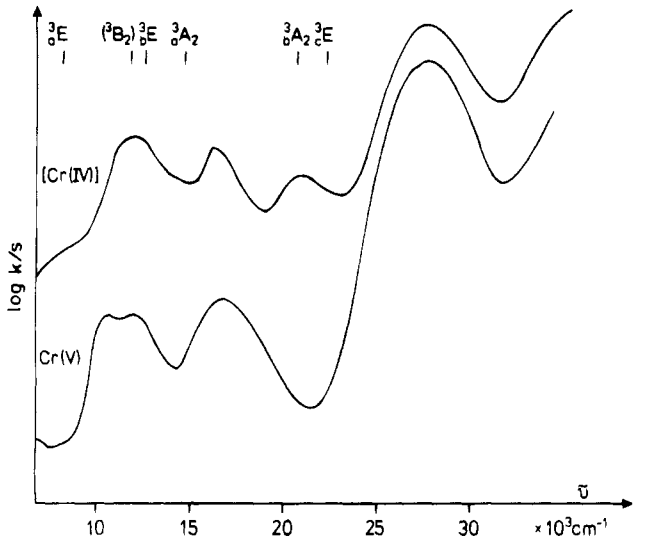

Figure 10. Diffuse reflectance spectrum (298 K, arbitrary intensity scale) of spodiosite type compounds $Ca_2(PO_4)_{1-x}(CrO_4)_xCl_{1-y}$: $x = 0.05$, $y = 0$, Cr(V), below; $x = 0.1$, $y < 0.1$; Cr(IV) (+Cr(V)), above. The band assignment is based on a model calculation with a tetragonally compressed tetrahedral geometry (118.5°) and the parameter set of Table 2 (only spin-allowed transitions are indicated; the $^3B_1(^3A_2) \rightarrow {}^3B_2(^3T_2)$ transition is symmetry forbidden).

Summary and Conclusions

Cr(IV) ions were successfully incorporated into the tetrahedral sites of various oxidic compounds with different structures, either by isomorphic substitution of Ge(IV) with a comparable ionic radius or—in the case of apatites and spodiosites—by an "in situ" reduction of Cr(V). Though it proved difficult to synthesize single crystals—due to a tendency to disproportionate into Cr(III) and Cr(V) in melts—pure Cr(IV)-doped solid powders were obtained. Most solids were free of impurities of chromium in other oxidation states, in contrast to most systems reported in literature so far. In some cases, mixed crystal series up to rather high chromium concentrations or even with complete miscibility could be prepared.

The chromium-doped oxidic solids were characterized mainly by optical spectroscopy in the spectral region of the d−d transitions. By fitting the band positions in the powder reflectance spectra on the basis of the host site geometries and utilizing an AOM program package, to our knowledge for the first time, we could obtain consistent and reliable ligand field parameters. The typical parameter set obtained for a CrO_4^{4-} tetrahedron with a Cr−O spacing of ≃1.77 Å is

$$\Delta \simeq 9650\ cm^{-1};\ B_{et} \simeq 480\ cm^{-1}\ (\beta_{et} \simeq 0.47)$$

$$(B_{ee} \simeq 530\ cm^{-1},\ B_{tt} < 480\ cm^{-1});\ C/B = 4.2$$

The B values differ because of symmetry-restricted covalency and are similar to those from an ab-initio calculation for the $Cr(OH)_4$ model complex. The derived parameter set is consistent with those reported for the isoelectronic Mn(V) and Fe(VI) cations in similar oxidic host structures. The band positions were rather insensitive with respect to the AOM parameters e_σ and e_π, so long as the correlated Δ value did not change.

The EPR spectra usually exhibit only an exchange-averaged signal with g_{eff} slightly below g_0. Apparently the isomorphic substitution of Cr(IV) into the host compounds occurs in clusters. Only rarely is the fine structure resolved, thus allowing an estimation of the zero-field-splitting parameters.

Single-crystal and luminescence spectra of Cr(IV)-doped oxidic compounds will be the subject of a separate paper.[21b]

Acknowledgment. The authors are grateful to Professor H.-H. Schmidtke and H. Adamsky (University Düsseldorf) for access to the AOM program package[30] and gratefully acknowledge the financial support of M.A. by the Humboldt Foundation.

IC940521L